Energy levels and transition rates of the laser-cooling candidate Th⁻

Rui Zhang ●, Yuzhu Lu ●, Shuaiting Yan, and Chuangang Ning ●*

Department of Physics, State Key Laboratory of Low Dimensional Quantum Physics,
Frontier Science Center for Quantum Information, Tsinghua University, Beijing 100084, China

The energy levels and transition rates of promising laser-cooling candidate thorium anion (Th⁻) are experimentally measured in the current work. Three excited states between the lower and upper states for the bound-bound electric dipole (E1) transition $^2S^o_{1/2} \leftrightarrow {}^4F^e_{3/2}$ of Th⁻ are observed: $^4G^o_{5/2}$, $^4F^e_{9/2}$, and $^4F^o_{7/2}$, and their energy levels are determined to be 1847(13), 3166.8(59), and 3666(12) cm⁻¹, respectively. Meanwhile, the lifetime of the upper state $^2S^o_{1/2}$ of the E1 transition is experimentally determined to be 30(2) μs, substantially shorter than the previously calculated result, which makes Th⁻ the most promising candidate for laser cooling of negative ions. Furthermore, the lifetimes of two other short-lived odd-parity excited states of Th⁻ are also measured to be 62(5) and 53(3) μs, respectively.

I. INTRODUCTION

Laser cooling [1,2], a crucial experimental technique for producing ultracold atoms and molecules, is opening up numerous new research areas [3,4] and enabling experiments at unprecedentedly low temperatures [5,6]. Initially achieved in positive ions Ba⁺ [7] and Mg⁺ [8] in 1978, the technique was later extended to neutral atom Na [9]. However, this promising technology has remained confined to neutral- and positive-ion systems, with no realization in any negative ion over the past half century. The primary obstacle is the lack of a closed and fast electric-dipole (E1) cycling transition between two bound states of opposite parity within a negative-ion system. In contrast to positive ions and neutral systems, which typically have nearly infinite bound states, negative ions possess their extra electrons due to the short-range polarization or electron correlation effects [10]. As a result, most atomic anions only have a single-configuration bound state [11–14]. Atomic negative ions with bound states of different configurations are rare, and the presence of E1 cycling transitions between these states is even more uncommon, as the E1 transitions can only occur between states of opposite parity. The molecular anion C_2^- has been proposed as a candidate for laser cooling [15–17]. However, molecular cooling requires the recycling of vibrational and rotational branching during the cycling transition, which complicates the laser systems involved.

Only four atomic anions (Os⁻ [18–23], Ce⁻ [24,25], La⁻ [22,26–29], and Th⁻ [30,31]) have been discovered to possess E1 transitions in the entire periodic table [14]. Among them, Ce⁻ has numerous metastable lower states, known as "dark states," between its bound-bound transition, making it less suitable for anionic laser cooling. The other three candidates each have their own strengths and weaknesses. Os⁻ was the first anion with an observed bound E1 transition [18]. The

wavelength of its laser-cooling transition was measured to be 1162.75 nm in the near-infrared range [20], which is comparatively more accessible than the midinfrared wavelengths of La⁻ (3103.7 nm) [27,29] and Th⁻ (2428.4 nm) [31]. However, our recent experiments determined the lifetime of the upper excited state of its E1 transition to be 201(10) μs [23], an order of magnitude slower than the theoretical rates of the other two candidate anions, La⁻ and Th⁻. La⁻ was calculated to have the fastest E1 transition rate at 4.9×10^4 s⁻¹ and the shortest cooling time of 1.2 s among all the candidates [29]. However, its stable isotope, ¹³⁹La⁻, with a nuclear spin of 7/2, has nine hyperfine components between its bound-bound cycling transition, requiring a complicated laser system for repumping [29].

For Th⁻, its potential laser-cooling transition is $^2S^o_{1/2} \leftrightarrow {}^4F^e_{3/2}$, and a few anionic bound states were predicted by the multiconfiguration Dirac-Hartree-Fock method in 2019 [30]. On the experimental side, the electron affinity of Th was determined to be 4901.35(48) cm⁻¹ using the cryo-SEVI spectrometer [30]. However, only some of the predicted bound states ($^4F^e_{3/2,5/2,7/2}$) were experimentally observed by the direct photodetachment [30]. In 2021, three electric-dipole transitions (T1, T2, and T3) from the ground state of Th⁻ to the short-lived odd-parity states were observed through a resonance scan [31]. T1 corresponds to the transition to the upper state $^2S^o_{1/2}$ of laser-cooling transition of Th⁻, with an energy level of 4118.0(10) cm⁻¹ above its ground state. T2 and T3 have been tentatively assigned to odd-parity states $^4F^o_{5/2}$ and $^4D^o_{1/2}$, with energies of 4592.6(10) and 4618.1(10) cm⁻¹, respectively. The complex electronic structure of Th⁻ remains incompletely understood, and several predicted states within the E1 transition range have yet to be observed. Further investigation is required to assess their impact on the optical cycling of Th⁻. The measured transition energies of transitions T1–T3 [31] could also be used to rescale their predicted lifetimes to be 73, 28, and 41 μs, respectively, according to

---

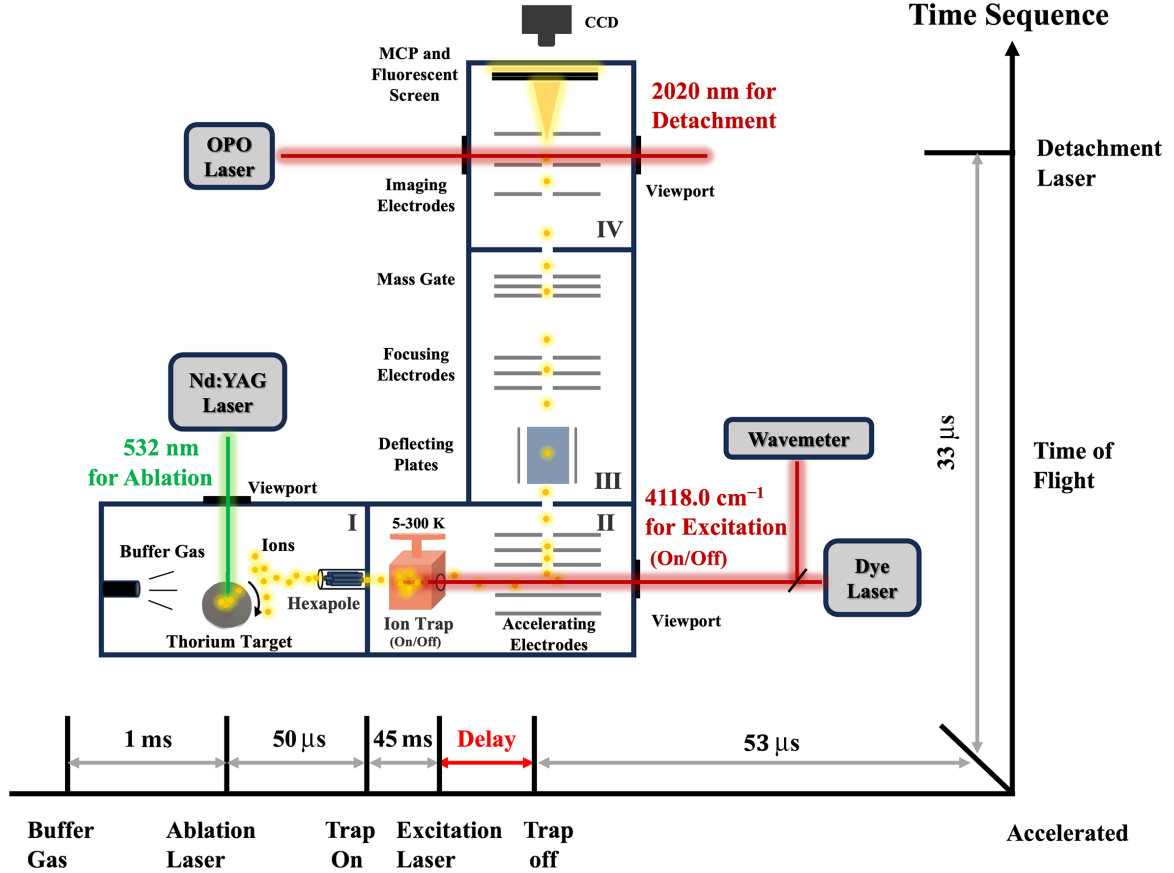*Contact author: ningcg@tsinghua.edu.cn

FIG. 1. Schematic view and the operation time sequence of our cryo-SEVI apparatus. It includes four main parts: (I) Ion source (Generating ions using laser ablation); (II) Cryogenic ion trap (Trapping and exciting ions); (III) The TOF mass spectrometer (Selecting Th^- anions); and (IV) Slow electron velocity-map imaging system (Measuring kinetic energies and angular distributions of photoelectrons). The yellow dots illustrate the trajectory of Th^-. The arrows outside the schematic show the operation time sequence. The time interval between the excitation laser on and the ion trap off, called "Delay" (in red), is adjusted to measure the lifetime of the excited states of Th^-. The decay of the excited Th^- during the fixed time interval 86 μs (53 + 33 μs) between the trap-off stage and the photodetachment experiment mainly deteriorates the S/N ratio, but does not affect the lifetime due to the exponential decay.

the relation $\tau \propto 1/E^3$. Here, E is the transition energy. The absence of experimental lifetime measurements underscores the need for ongoing research.

In the present work, we report the observation of three bound excited states of Th^- ($^4G^o_{5/2}$, $^4F^e_{9/2}$, and $^4F^o_{7/2}$) by extending the range of our detachment laser into the infrared band. The relatively long lifetime of the $^2S^o_{1/2}$ state of Th^- (~a few tens of microseconds) renders the typical pump-probe method unfeasible. By utilizing a cold-ion trap, the first pulsed laser excites Th^- in the ion trap, and, after an adjustable delay, a second pulsed laser measures the population of the excited states using photoelectron energy spectroscopy. The lifetimes of three short-lived odd-parity excited states of Th^- are successfully measured with this method.

II. EXPERIMENT METHODS

In brief, our cryo-SEVI apparatus has four main parts: an ion source for producing ions, a cryogenic ion trap for trapping anions, a time-of-flight (TOF) mass spectrometer for selecting Th^-, and a velocity-map imaging system for acquiring photoelectron energy spectra [31–34], as shown in Fig. 1. A pulsed 532-nm Nd: yttrium aluminum garnet laser is focused

onto a thorium metal target to produce ions in the source chamber. The resulting negative ions are guided by a hexapole and trapped in the radio-frequency (rf) octupole cryogenic ion trap [35], where they are cooled down to a nominal temperature of a few K via the collisions with the buffer gas (H_2 or He) delivered by a pulsed valve. The typical trapping period is ~45 ms. A midinfrared laser at 2428.4 nm (4118.0 cm^{-1}) from a difference-frequency generation (DFG) system is used to excite Th^- from the ground $^4F^e_{3/2}$ state to the $^2S^o_{1/2}$ state in the cryogenic ion trap through a CaF_2 view window. The DFG system covers an infrared tuning range of $1.5 - 4.2$μm, achieved with a dye laser (Spectra-Physics, linewidth ~0.06 cm^{-1}) and its residual fundamental 1064-nm output. The wavelength and intensity are monitored by a wavelength meter (HighFinesse WS6-600) with an accuracy of 0.02 cm^{-1}. After an adjustable delay, the excited Th^- ions are ejected from the ion trap for population analysis using the photoelectron energy spectroscopy. Given that the time of flight in the TOF mass spectrometer [36] is a fixed value for Th^-, the adjustable *delay time* (the time interval between the excitation laser fired on and the ion trap ejection) is used to measure the lifetime of the excited states of Th^- (see Fig. 1). This method was also used in measurements of the excited-state lifetime

of Os$^-$ [23]. To minimize the deexcitation of the excited Th$^-$ during the time of flight, the acceleration voltage of TOF is increased from 1 to 3 kV, resulting in a reduction of the TOF time from 57 to 33 µs. The ejection voltage of the ion trap is also increased to reduce the time of excited Th$^-$ to reach the accelerating electrodes. In the velocity-imaging system [37,38], an optical parametric oscillator (OPO) laser (Spectra-Physics primoScan, $400 - 2700$ nm, linewidth $\sim$6 cm^{-1}) and the dye laser ($400 - 920$ nm) are used for the photodetachment to measure the energy levels of Th$^-$. The apparatus operates at a repetition rate of 20 Hz.

The distributions of detached photoelectrons are reconstructed using the maximum entropy velocity Legendre reconstruction method [39,40]. Since the detached electrons with the same velocity form a spherical shell with the same radius (r), its kinetic energy (E_k) can be given by $E_k = \alpha r^2$, where α is the calibration coefficient of the spectrometer. The radius r is determined by Gaussian function fitting of the center position of each peak. The energy levels obtained at different photon energies are further optimized using a global optimization analysis [41,42].

III. RESULTS AND DISCUSSION

A. Three newly observed bound states

Figure 2 shows photoelectron spectra of Th$^-$ obtained through direct detachment at different photodetachment wavelengths. The energy spectrum in black was acquired at photon energy 11 603.57 cm^{-1} using the dye laser, while the others were recorded using the OPO laser. The strongest peak, peak 9, is the transition from the anionic ground state to the neutral ground state, and its binding energy is measured to be 4902.6(61) cm^{-1}, consistent with the previous result of the electron affinity (EA) of Th atom [30]. At lower photon energies, the relative intensity of EA peak 9 is suppressed according to the Wigner threshold law and peaks became sharp thanks to the feature of Slow Electron Velocity–Mapping Imaging (SEVI), allowing additional weaker peaks 4–7 to be resolved. Peaks 4 and 5 have similar photoelectron kinetic energies but exhibit distinctly different photoelectron angular distributions, suggesting that their initial anionic states possess opposite parities. Since peak 5 has been identified as the transitions from the anionic excited state Th$^-$ ($^4F^e_{5/2}$) to the atomic ground state Th ($^3F_2$) [30], peak 4 is assigned to the transition from the lowest anionic odd-parity state Th$^-$ ($^4G^o_{5/2}$) to the same neutral state Th ($^3F_2$) now. This transition was predicted by high-precision calculations [30] and had not been experimentally observed previously due to the resolution limitation. To assign other observed peaks, we varied the trap time to analyze the intensity trends of the different peaks. The intensity of a peak originating from an excited state with a shorter lifetime exhibits faster intensity decay with increasing trap time. We collected a series of energy spectra with different trapped time (blue curve for 45 ms, purple for 5 ms), and the no-trap mode (red for no trap). Peaks 1 and 6 correspond to the transitions from the newly observed anionic state $^4F^o_{7/2}$. Peak 3 was previously assigned as the transition from the long-lived anionic excited state Th$^-$ ($^4F^e_{7/2}$) [30]. Peaks 2, 7, and 10 are now assigned to the transitions from the
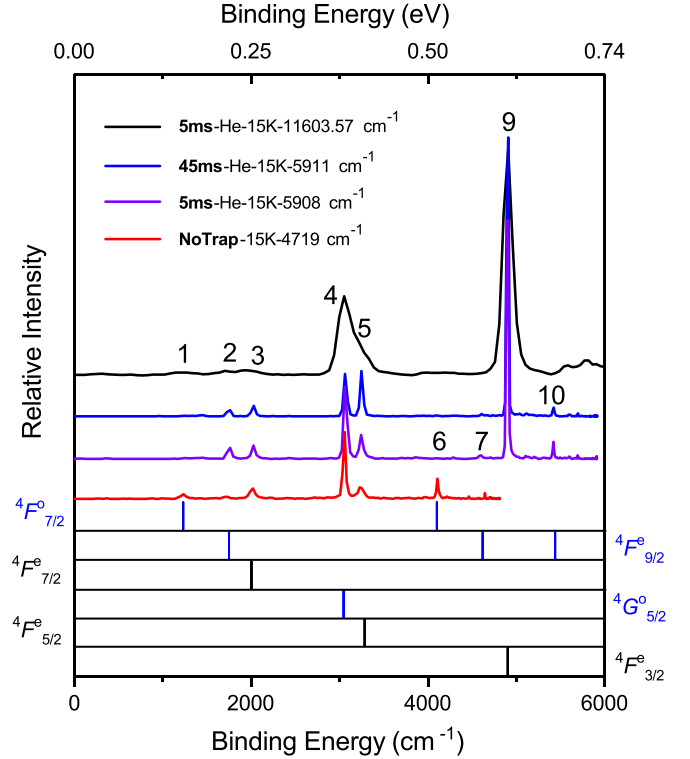

FIG. 2. The photoelectron spectra of Th$^-$ observed at the different photon energies and trapped times. The assignment of each transition is listed in Table I. Three sets of blue sticks below the spectra indicate the energy levels of the final neutral states from the three newly identified states of Th$^-$. The other three sets of black sticks indicate those from the previously assigned anionic states $^4F^e_{3/2,5/2,7/2}$ of Th$^-$. Note that the weak peak 8 is invisible at the photon energy 11 603.57 cm^{-1} due to the very small energy gap 20 cm^{-1} between peaks 8 and 9 and the overwhelming intensity of strong peak 9.

same newly observed anionic state $^4F^e_{9/2}$ to different neutral Th states. Note that the peak 8 near peak 9 in Fig. 3 is a transition from Th$^-$ ($^4F^e_{7/2}$) to Th ($^3F_3$), with a measured binding energy of 4878.8(61) cm^{-1}. The energy gap between peaks 8 and 9 is only 20 cm^{-1}, highlighting the high resolution near the photodetachment threshold. Since the binding energy of the transition 8 is precisely measured near the threshold, the energy level of the anionic state $^4F^e_{7/2}$ is also updated to a more accurate value to be 2892.9(50) cm^{-1} through global optimization analysis. The binding energies and assignments of all observed peaks are listed in Table I. The three newly identified anionic excited states are illustrated in Fig. 4 and listed in Table II.

B. Transition rate of the laser-cooling cycle

To determine the transition rate of the laser-cooling transition $^2S^o_{1/2} \leftrightarrow {}^4F^e_{3/2}$, we measured the lifetime of the upper state $^2S^o_{1/2}$ via the E1 transition. As shown in Fig. 3(a), no peak from $^2S^o_{1/2}$ can be observed through the single-photon direct photodetachment due to its low population and a short lifetime predicted to be a few tens of microseconds [31]. To observe this short-lived state, a DFG laser with a photon energy 4118.0 cm^{-1} was used to excite Th$^-$ to the state
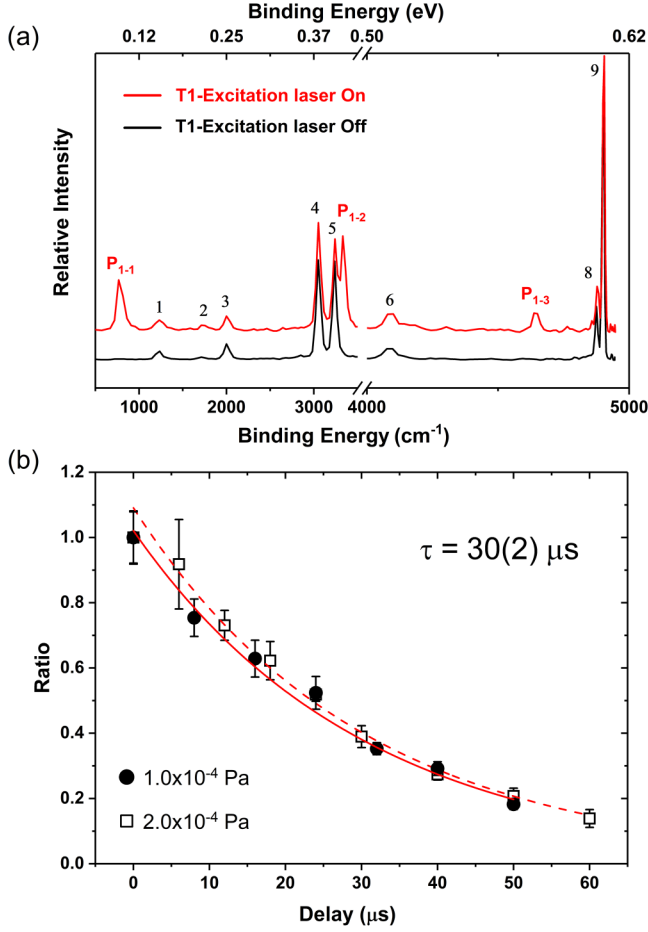
FIG. 3. (a) The photoelectron energy spectra of Th$^-$ with (in red) and without (in black) the excitation laser at 4118.0 cm^{-1}. The photon energy of the detachment laser is 4947 cm^{-1}. Red peaks $P_{1-1,2,3}$ are the transitions from the odd-parity excited state $^2S^o_{1/2}$ of Th$^-$. The delay time used for the displayed "laser on" photoelectron spectrum is 0 µs. (b) The intensity ratio of peak P_{1-1} Th($^3F_2$) ← Th$^-$ ($^2S^o_{1/2}$) to peak 9 Th($^3F_2$) ← Th$^-$ ($^4F^e_{3/2}$) vs the delay time. The red solid and dash lines are the fitting curve according to the equation $I(t) = I_0 e^{-t/\tau}$. The lifetime of $^2S^o_{1/2}$ state is measured to be 30(2) µs at the background pressure of both 1.0×10^{-4} and 2.0×10^{-4} Pa.

$^2S^o_{1/2}$. Three emerging peaks labeled P_{1-1}, P_{1-2}, and P_{1-3} were successfully observed, as illustrated by the red curve in Fig. 3. These new peaks are from the excited state $^2S^o_{1/2}$ to the different final neutral states. All assigned transitions are listed in Table I. The relative intensities of these peaks from $^2S^o_{1/2}$ decrease gradually when increasing the delay time due to the spontaneous emission. To compensate for the fluctuation of the ion-beam intensity, we recorded the intensity ratio $I(t)$ of peak P_{1-1} to strong peak 9 versus the delay time t (defined in the Experiment Methods). The lifetime τ of $^2S^o_{1/2}$ state is determined to be 30(2) µs via exponential decay fitting of $I(t) = I_0 e^{-t/\tau}$ to the observed results, as shown in Fig. 3(b). Note that the exponential decay is a simplified representation of the time evolution of the intensity ratios, as the population in the excited state is estimated to be only 0.5% or less at the photodetachment zone, which is significantly smaller than the population in the ground state. The mean free time

of the buffer gas (H$_2$) collisions in the ion trap at the end of trapping is estimated to be 5 ms, much longer than the measured lifetime. To experimentally assess the impact of collisions on the lifetime, we reduced the gas density in the ion trap by monitoring the background pressure of the chamber from 2×10^{-4} to 1×10^{-4} Pa, and the lifetime remained at 30(2) µs [see Fig. 3(b)], indicating that collision effects are negligible. In addition, we measured the lifetimes of the other two short-lived odd-parity states ($^4F^o_{5/2}$ and $^4D^o_{1/2}$) of Th$^-$ via

TABLE I. Binding energies of observed transitions in the present work.

Label	Level (Th$^-$ → Th)[a]	Measured binding energy (cm^{-1})	Optimized binding energy (cm^{-1})[b]
P_{3-1}	$^4D^o_{1/2} \to {}^3F^e_2$	287(49)	283(11)
P_{2-1}	$^4F^o_{5/2} \to {}^3F^e_2$	304(50)	304(50)
P_{1-1}	$^2S^o_{1/2} \to {}^3F^e_2$	782(23)	783.1(11)
1	$^4F^o_{7/2} \to {}^3F^e_2$	1234(21)	1235(12)
2	$^4F^e_{9/2} \to {}^3F^e_2$	1738(20)	1734.5(59)
3	$^4F^e_{7/2} \to {}^3F^e_2$	2007(17)	2008.4(50)
4	$^4G^o_{5/2} \to {}^3F^e_2$	3054(12)	3054(12)
P_{3-2}	$^4D^o_{1/2} \to {}^3F^e_2$	3166(22)	3152(11)
5	$^4F^e_{5/2} \to {}^3F^e_2$	3241(11)	3244(6)
P_{1-2}	$^2S^o_{1/2} \to {}^3P^e_0$	3334(11)	3341.2(11)
P_{3-3}	$^4D^o_{1/2} \to {}^3P^e_2$	3966(13)	3971(11)
6	$^4F^o_{7/2} \to {}^3F^e_3$	4105(14)	4104(12)
7	$^4F^e_{9/2} \to {}^3F^e_3$	4596(12)	4603.6(59)
P_{1-3}	$^2S^o_{1/2} \to {}^3P^e_1$	4643.4(63)	4648.6(11)
8	$^4F^e_{7/2} \to {}^3F^e_3$	4878.8(61)	4877.5(50)
9	$^4F^e_{3/2} \to {}^3F^e_2$	4902.6(61)	4901.35(48)
10	$^4F^e_{9/2} \to {}^3P^e_2$	5424.7(71)	5422.5(59)

[a]The electronic configuration of Th$^-$ is $6d^3 7s^2$ (even parity) or $6d^2 7s^2 7p$ (odd parity).
[b]The optimized binding energy values are deduced according to the assignments, the measured binding energy of each transition, and the energy levels of the neutral Th [45] using a global optimization.

TABLE II. Summary of the measured and calculated energy levels of Th$^-$ anion.

State of Th$^-$ [a]	Measured energy level (cm^{-1})	Calculated energy level (cm^{-1}) [b]	Reference
$^4F^e_{3/2}$	0	0	Tang *et al.* [30]
$^4F^e_{5/2}$	1657(6)	1377	
$^4G^o_{5/2}$	1847(13)	401	This work
$^4F^e_{7/2}$	2892.9(50)	2642	
$^4F^e_{9/2}$	3166.8(59)	3637	
$^4F^o_{7/2}$	3666(12)	3974	
$^2S^o_{1/2}$	4118.0(10)	3904	Tang *et al.* [31]
$^4F^o_{5/2}$	4592.6(10)	3992	
$^4D^o_{1/2}$	4618.1(10)	4503	

[a]The superscripts *e* and *o* indicate the state parity of Th$^-$: even parity $6d^3 7s^2$ and odd parity $6d^2 7s^2 7p$.
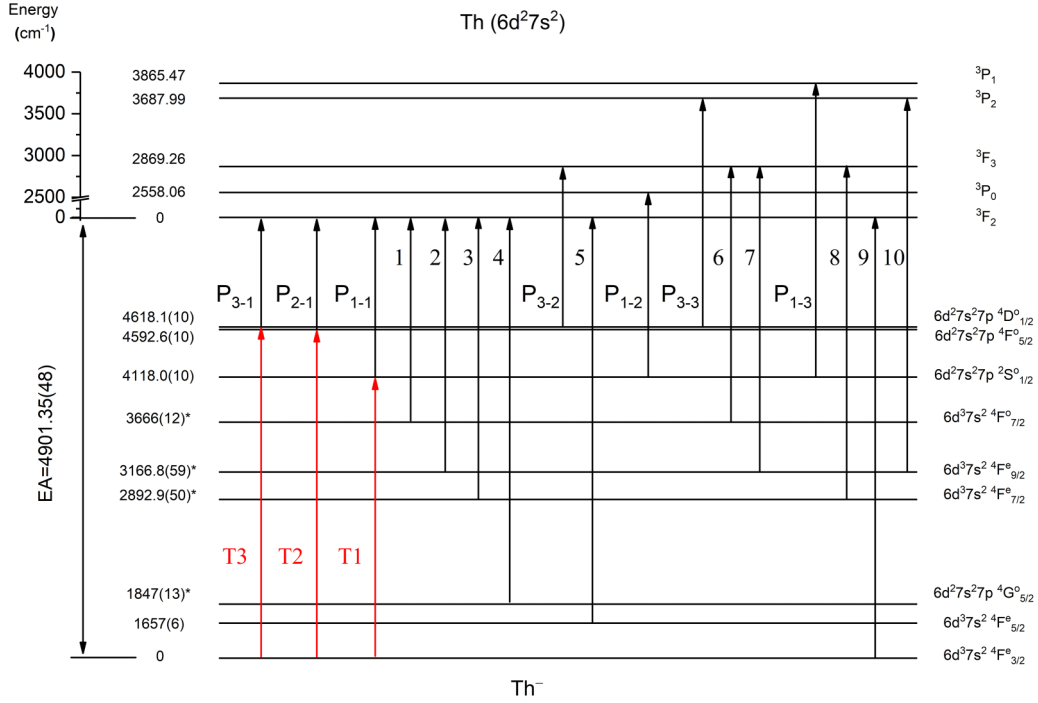[b]The calculated energy levels of Th$^-$ are quoted from Refs. [30,31].

FIG. 4. The related energy levels of Th$^-$ and Th. Labels of transitions are the same as the observed peaks in other figures. Three red arrows represent the excitation process used to measure the lifetime of the upper state for the transitions T1–T3. The data of energy levels with asterisk are determined in the present work.

the excitation processes T2 and T3, determining their lifetime to be 62(5) and 53(3) μs, respectively, as shown in Fig. 5. The summary of the lifetime data of these three odd-parity states is presented in Table III.

C. Discussion on laser-cooling candidate Th$^-$

With the energy levels and lifetimes of the laser-cooling candidate Th$^-$ further experimentally determined, we update the calculations related to its laser-cooling here. For the three newly observed excited states between the cooling-cycle transition $^2S^o_{1/2} \leftrightarrow \, ^4F^e_{3/2}$: $^4G^o_{5/2}$, $^4F^e_{9/2}$, and $^4F^o_{7/2}$, the transitions from the state $^2S^o_{1/2}$ to these states are E2, M4, and M3 types, respectively. These transitions are expected to be too weak to break the closure of the E1 laser-cooling cycle. With the updated lifetime of the upper state $^2S^o_{1/2}$ at 30(2) μs, the transition rate is calculated to be $3.3(2) \times 10^4$ s^{-1}, substan-

tially faster than previous predictions [31], making Th$^-$ a most promising candidate for the laser cooling of negative ions. The laser-cooling period T is shortened from 7.8 to 2.7 s, while the natural linewidth $\Delta \nu$ of this transition increases from 1.9 to 5.4 kHz. The photodetachment loss rate, $\propto \Delta \nu T$, remains negligible at 0.025% [31]. The only stable isotope ^{232}Th, with zero nuclear spin, has no hyperfine splitting in its cooling transition, greatly simplifying the cooling laser system compared to ^{139}La$^-$. Comparison of all atomic anion laser-cooling candidates can be found in Table IV. A current challenge for Th$^-$ is the difficulty in obtaining a stable mid-infrared laser with a narrow linewidth (2428.4 nm). We plan to use external-cavity diode lasers to address this issue. In principle, once Th$^-$ anions are effectively cooled, any other negatively charged species can be cooled down using the sympathetic cooling [19,43,44]. Combined with the threshold photodetachment [23], a variety of cold neutral atoms and molecules could also be produced.

IV. CONCLUSIONS

In summary, we measured the lifetime of the upper state for E1 transition of laser-cooling candidate Th$^-$ to be 30(2) μs. This result reveals a laser-cooling rate that is substantially faster than previously predicted [31]. We also measured the lifetimes of two other short-lived odd-parity excited states as 62(5) and 53(3) μs, respectively. The complex energy levels of the Th$^-$ anion have now been further clarified, with the observation of three new excited states $^4G^o_{5/2}$, $^4F^e_{9/2}$, and $^4F^o_{7/2}$. Our results on energy levels and lifetimes of the thorium anions demonstrate the existence of a closed and fast

TABLE III. Summary of the lifetimes (τ) in μs, transition energies (E) in cm^{-1}, and rates (A) in s^{-1} of three observed odd-parity excited states of Th$^-$. T1 is the laser-cooling transition cycle $^2S^o_{1/2} \leftrightarrow \, ^4F^e_{3/2}$ of Th$^-$. Numbers in brackets for the transition rate A represent the power of 10.

Transition	Type	E	A	τ (Expt.)	τ (Theo.) [a]
T1($^2S^o_{1/2} \leftrightarrow \, ^4F^e_{3/2}$)	E1	4118.0	3.33 [4]	30(2)	73
T2	E1	4592.6	1.69 [4]	62(5)	28
T3	E1	4618.1	1.89 [4]	53(3)	41

[a]The measured transition energies of T1–T3 have been used to rescale the predicted lifetime τ according to $\tau \propto 1/E^3$.
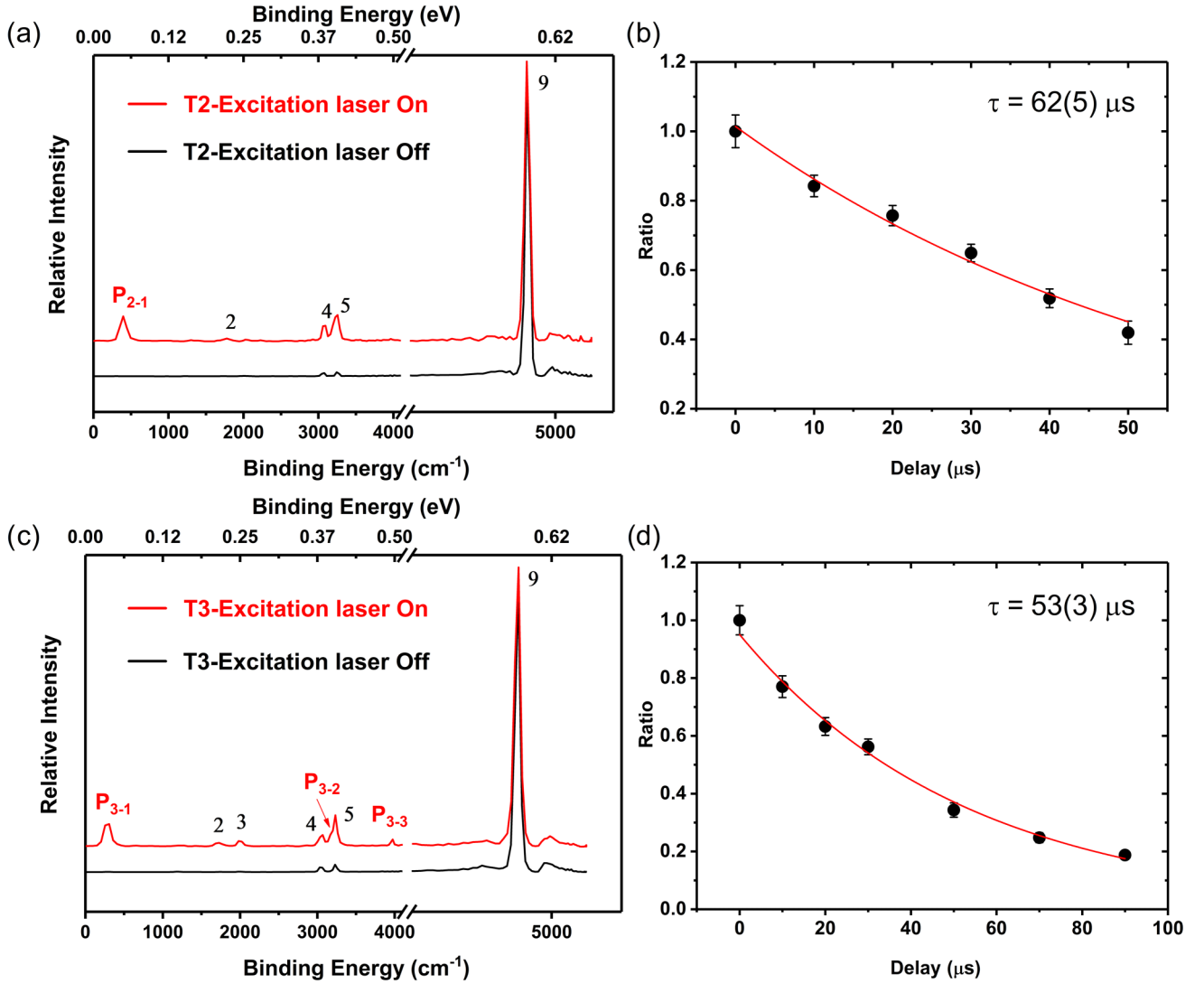
FIG. 5. The photoelectron energy spectra of Th$^-$ with (in red) and without (in black) the excitation laser at 4592.6 cm^{-1} (a), T2, and 4618.1 cm^{-1} (c), T3. The photon energies of detachment lasers are 5124 (T2) and 5098 cm^{-1} (T3), respectively. The delay times used for the displayed "laser on" photoelectron spectra are 0 μs. The intensity ratios of peaks P_{2-1} (b) and P_{3-1} (d) to peak *9* vs the delay time. The lifetimes of these two odd-parity states are measured to be 62(5) and 53(3) μs, respectively.

E1 transition, strongly supporting Th$^-$ as a promising candidate for laser cooling of negative ions. Furthermore, these experimental results also provide a benchmark for the development of high-precision theoretical calculations for heavy elements.

TABLE IV. Comparison of three anionic laser-cooling candidates (see below)[a].

Anion	Lifetime (μs)	Transition rate (s^{-1})	Wavelength (nm)	Frequency (THz)	Cooling time (s)	Repumping laser	Nuclear spin
Th$^-$	30(2)	3.3×10^4	2428.4	123.455	2.8	0	0
Os$^-$	201(10)	5.0×10^3	1162.8	257.831	4.7	1	0
La$^-$	20.4(2.1)	4.9×10^4	3103.7	96.593	1.2	5[b]	7/2

[a]Please note these candidates are shown in Refs. [18–23,26–31].
[b]Reference [27] suggested one repumping laser with a wide linewidth to repump three hyperfine levels of the ground state (1487, 1484, and 1455 MHz). However, a wideband laser may lead to a significant photodetachment loss.

[1] A. Ashkin, Trapping of atoms by resonance radiation pressure, Phys. Rev. Lett. **40**, 729 (1978).

[2] W. D. Phillips, Nobel lecture: Laser cooling and trapping of neutral atoms, Rev. Mod. Phys. **70**, 721 (1998).

[3] C. E. Wieman, D. E. Pritchard, and D. J. Wineland, Atom cooling, trapping, and quantum manipulation, Rev. Mod. Phys. **71**, S253 (1999).

[4] A. D. Cronin, J. Schmiedmayer, and D. E. Pritchard, Optics and interferometry with atoms and molecules, Rev. Mod. Phys. **81**, 1051 (2009).

[5] T. K. Langin, G. M. Gorman, and T. C. Killian, Laser cooling of ions in a neutral plasma, Science **363**, 61 (2019).

[6] D. S. Jin and J. Ye, Introduction to ultracold molecules: New frontiers in quantum and chemical physics, Chem. Rev. **112**, 4801 (2012).

[7] W. Neuhauser, M. Hohenstatt, P. Toschek, and H. Dehmelt, Optical-sideband cooling of visible atom cloud confined in parabolic well, Phys. Rev. Lett. **41**, 233 (1978).

[8] D. J. Wineland, R. E. Drullinger, and F. L. Walls, Radiation-pressure cooling of bound resonant absorbers, Phys. Rev. Lett. **40**, 1639 (1978).

[9] S. Chu, L. Hollberg, J. E. Bjorkholm, A. Cable, and A. Ashkin, Three-dimensional viscous confinement and cooling of atoms by resonance radiation pressure, Phys. Rev. Lett. **55**, 48 (1985).

[10] T. Andersen, Atomic negative ions: Structure, dynamics and collisions, Phys. Rep. **394**, 157 (2004).

[11] H. Hotop and W. C. Lineberger, Binding energies in atomic negative ions, J. Phys. Chem. Ref. Data **4**, 539 (1975).

[12] H. Hotop and W. C. Lineberger, Binding energies in atomic negative ions: II, J. Phys. Chem. Ref. Data **14**, 731 (1985).

[13] T. Andersen, H. K. Haugen, and H. Hotop, Binding energies in atomic negative ions: III, J. Phys. Chem. Ref. Data **28**, 1511 (1999).

[14] C. Ning and Y. Lu, Electron affinities of atoms and structures of atomic negative ions, J. Phys. Chem. Ref. Data **51**, 021502 (2022).

[15] P. Yzombard, M. Hamamda, S. Gerber, M. Doser, and D. Comparat, Laser cooling of molecular anions, Phys. Rev. Lett. **114**, 213001 (2015).

[16] M. Nötzold, R. Wild, C. Lochmann, and R. Wester, Spectroscopy and ion thermometry of C_2^- using laser-cooling transitions, Phys. Rev. A **106**, 023111 (2022).

[17] M. Nötzold, R. Wild, C. Lochmann, T. Rahim, S. Purushu Melath, K. Dulitz, B. Mant, J. Franz, F. A. Gianturco, and R. Wester, Vibrational quenching of optically pumped carbon dimer anions, Phys. Rev. Lett. **131**, 183002 (2023).

[18] R. C. Bilodeau and H. K. Haugen, Experimental studies of Os⁻: Observation of a bound-bound electric dipole transition in an atomic negative ion, Phys. Rev. Lett. **85**, 534 (2000).

[19] A. Kellerbauer and J. Walz, A novel cooling scheme for antiprotons, New J. Phys. **8**, 45 (2006).

[20] U. Warring, M. Amoretti, C. Canali, A. Fischer, R. Heyne, J. O. Meier, C. Morhard, and A. Kellerbauer, High-resolution laser spectroscopy on the negative osmium ion, Phys. Rev. Lett. **102**, 043001 (2009).

[21] A. Fischer, C. Canali, U. Warring, A. Kellerbauer, and S. Fritzsche, First optical hyperfine structure measurement in an atomic anion, Phys. Rev. Lett. **104**, 073004 (2010).

[22] L. Pan and D. R. Beck, Candidates for laser cooling of atomic anions: La⁻ versus Os⁻, Phys. Rev. A **82**, 014501 (2010).

[23] Y. Lu, R. Zhang, C. Song, C. Chen, R. Si, and C. Ning, Energy levels and transition rates for laser cooling Os⁻ and a general approach to produce cold atoms and molecules, Chin. Phys. Lett. **40**, 093101 (2023).

[24] C. W. Walter, N. D. Gibson, C. M. Janczak, K. A. Starr, A. P. Snedden, R. L. Field III, and P. Andersson, Infrared photodetachment of Ce⁻: Threshold spectroscopy and resonance structure, Phys. Rev. A **76**, 052702 (2007).

[25] C. W. Walter, N. D. Gibson, Y.-G. Li, D. J. Matyas, R. M. Alton, S. E. Lou, R. L. Field, D. Hanstorp, L. Pan, and D. R. Beck, Experimental and theoretical study of bound and quasibound states of Ce⁻, Phys. Rev. A **84**, 032514 (2011).

[26] C. W. Walter, N. D. Gibson, D. J. Matyas, C. Crocker, K. A. Dungan, B. R. Matola, and J. Rohlén, Candidate for laser cooling of a negative ion: Observations of bound-bound transitions in La⁻, Phys. Rev. Lett. **113**, 063001 (2014).

[27] E. Jordan, G. Cerchiari, S. Fritzsche, and A. Kellerbauer, High-resolution spectroscopy on the laser-cooling candidate La⁻, Phys. Rev. Lett. **115**, 113001 (2015).

[28] A. Kellerbauer, G. Cerchiari, E. Jordan, and C. W. Walter, High-resolution laser spectroscopy on bound–bound transitions in La⁻, Phys. Scr. **90**, 054014 (2015).

[29] G. Cerchiari, A. Kellerbauer, M. S. Safronova, U. I. Safronova, and P. Yzombard, Ultracold anions for high-precision antihydrogen experiments, Phys. Rev. Lett. **120**, 133205 (2018).

[30] R. Tang, R. Si, Z. Fei, X. Fu, Y. Lu, T. Brage, H. Liu, C. Chen, and C. Ning, Candidate for laser cooling of a negative ion: High-resolution photoelectron imaging of Th⁻, Phys. Rev. Lett. **123**, 203002 (2019).

[31] R. Tang, R. Si, Z. Fei, X. Fu, Y. Lu, T. Brage, H. Liu, C. Chen, and C. Ning, Observation of electric-dipole transitions in the laser-cooling candidate Th⁻ and its application for cooling antiprotons, Phys. Rev. A **103**, 042817 (2021).

[32] X. Chen and C. Ning, Accurate electron affinity of Co and fine-structure splittings of Co⁻ via slow-electron velocity-map imaging, Phys. Rev. A **93**, 052508 (2016).

[33] R. Tang, X. Fu, and C. Ning, Accurate electron affinity of Ti and fine structures of its anions, J. Chem. Phys. **149**, 134304 (2018).

[34] R. Zhang, Y. Lu, R. Tang, and C. Ning, Electron affinity of atomic scandium and yttrium and excited states of their negative ions, J. Chem. Phys. **158**, 084303 (2023).

[35] J. B. Kim, M. L. Weichman, and D. M. Neumark, Low-lying states of FeO and FeO⁻ by slow photoelectron spectroscopy, Mol. Phys. **113**, 2105 (2015).

[36] W. C. Wiley and I. H. McLaren, Time-of-flight mass spectrometer with improved resolution, Rev. Sci. Instrum. **26**, 1150 (2004).

[37] I. León, Z. Yang, H.-T. Liu, and L.-S. Wang, The design and construction of a high-resolution velocity-map imaging apparatus for photoelectron spectroscopy studies of size-selected clusters, Rev. Sci. Instrum. **85**, 083106 (2014).

[38] A. T. J. B. Eppink and D. H. Parker, Velocity map imaging of ions and electrons using electrostatic lenses: Application in photoelectron and photofragment ion imaging of molecular oxygen, Rev. Sci. Instrum. **68**, 3477 (1997).

[39] B. Dick, Inverting ion images without Abel inversion: Maximum entropy reconstruction of velocity maps, Phys. Chem. Chem. Phys. **16**, 570 (2014).

[40] B. Dick, MELEXIR: Maximum entropy Legendre expanded image reconstruction. A fast and efficient method for the analysis of velocity map imaging or photoelectron imaging data, Phys. Chem. Chem. Phys. **21**, 19499 (2019).

[41] L. J. Radziemski, K. J. Fisher, D. W. Steinhaus, and A. S. Goldman, Calculation of atomic energy level values, Comput. Phys. Commun. **3**, 9 (1972).

[42] A. E. Kramida, The program LOPT for least-squares optimization of energy levels, Comput. Phys. Commun. **182**, 419 (2011).

[43] S. M. O'Malley and D. R. Beck, Lifetimes and branching ratios of excited states in La⁻, Os⁻, Lu⁻, Lr⁻, and Pr⁻, Phys. Rev. A **81**, 032503 (2010).

[44] S. Willitsch, M. T. Bell, A. D. Gingell, S. R. Procter, and T. P. Softley, Cold reactive collisions between laser-cooled ions and velocity-selected neutral molecules, Phys. Rev. Lett. **100**, 043203 (2008).

[45] J. E. Sansonetti and W. C. Martin, Handbook of basic atomic spectroscopic data, J. Phys. Chem. Ref. Data **34**, 1559 (2005).